Theor Appl Climatol (2012) 107:461–477
DOI 10.1007/s00704-011-0486-9

ORIGINAL PAPER

Calculating downward longwave radiation under clear and cloudy conditions over a tropical lowland forest site: an evaluation of model schemes for hourly data

Toby R. Marthews · Yadvinder Malhi · Hiroki Iwata

Received: 7 May 2011 / Accepted: 5 July 2011 / Published online: 28 July 2011

Abstract Field measurements of radiation fluxes—notably downwelling longwave radiation flux (LW flux)—are as yet rare or nonexistent outside a very select number of sites in the tropics. Data gaps can only be filled through the use of estimation schemes based on measurements of other meteorological variables, and there is a need for recommendations on best practice in this area. We selected 18 contrasting semi-empirical estimation schemes for downward longwave radiation, based on air emissivities, combined with six different sky cover estimation schemes and compared the expected longwave flux with hourly observations from a flux tower at Caxiuanã in Brazil. Of all schemes tested, the Dilley–Kimball emissivity scheme combined with Kasten and Czeplak's sky cover scheme during the day and Dilley and O'Brien's model B scheme at night proved to be the most reliable, yielding estimates of LW flux generally within 20 W/m^2 of measurements across all time points.

1 Introduction

Atmospheric longwave (LW) downward irradiance, L_d, is one of the major components of the energy balance of forest ecosystems (Monteith and Unsworth 1990; Crawford and Duchon 1999; Malhi et al. 2002a; Iziomon et al. 2003; IPCC 2007). In a forest, L_d is received by the upper surface of the canopy and, through its influence on canopy leaf temperatures, strongly influences several key ecosystem variables including photosynthetic rate, plant respiration and primary productivity (Leigh 1999; Jones et al. 2004). Values of L_d at any particular time and place are controlled by shortwave (SW) irradiance, cloud cover, cloud type and depth, as well as ambient values of vapour pressure, temperature and atmospheric precipitable water. Despite the well-known importance of all these quantities for the ecology of lowland tropical forests, it is still rare for L_d and related variables to be measured in situ at meteorological stations (Stöckli 2007; Okogbue et al. 2009), partly because of instrumentation costs and difficulty of access to many areas (Restrepo-Coupe et al., in preparation). Across the tropics, the distribution of meteorological stations is much less dense than in the temperate and boreal zones (Peel et al. 2007), and at the same time, the importance of L_d for the energetic functioning of tropical moist biomes is higher because cloudless days are generally the exception rather than the rule (Leigh 1999; Gabathuler et al. 2001) and closer to the Equator seasonal sun-angle variation is reduced, which means that cloudiness becomes a relatively more important determinant of incoming radiation conditions (Malhi et al. 2002b). The importance of the diffuse fraction of atmospheric radiation for forest productivity and carbon balance is becoming increasingly well known (Mercado et al. 2009; Kanniah et al. 2010), so the need for an improved measurement network for incident radiation is apparent.

Over recent years, much effort has been invested in the development of automatic networks for the long-term measurement of meteorological and radiation variables relevant to longwave flux (e.g. the Baseline Surface

CAPSULE: We used air emissivity and sky cover data from a tropical forest in Eastern Amazonia to compare schemes for estimating downwelling longwave irradiance, and we make recommendations for gap-filling meteorological data used in vegetation models.

T. R. Marthews (✉) · Y. Malhi
Environmental Change Institute,
School of Geography and the Environment, University of Oxford,
Oxford OX1 3QY, UK
e-mail: Toby.Marthews@ouce.ox.ac.uk

H. Iwata
International Arctic Research Center,
University of Alaska Fairbanks,
Fairbanks, AK 99775, USA

Radiation Network, http://www.bsrn.awi.de/; Global Monitoring Division Radiation Group, http://www.esrl.noaa.gov/gmd/grad/; the AErosol RObotic NETwork, http://aeronet.gsfc.nasa.gov/; Global Atmosphere Watch, http://gaw.empa.ch/gawsis/). L_d is also routinely measured at some micrometeorological flux tower sites, so the expansion of the worldwide flux tower network in recent years has been very welcome (e.g. FLUXNET, http://daac.ornl.gov/FLUXNET/; Baldocchi et al. 2001). Good radiation data are essential not only for ecological and climate studies but also for agricultural practice and food production, for the development of solar renewable energy systems, for crop simulation models and for the characterisation of land surface processes in general (Ellingson 1995; IPCC 2007). The sensitivity of L_d to changes in atmospheric greenhouse gas concentration also makes it an important indicator variable for climate change (Wild 2008), and through atmospheric feedbacks such as the possible increase in Amazonian rainfall as a consequence of accelerated biomass burning (Lin et al. 2006; Kanniah et al. 2010), cloud cover and aerosol load can also serve as good indicators of other societal changes. However, availability of good, long-term data on L_d and related variables remains extremely patchy (Gabathuler et al. 2001; Muneer et al. 2004; Stöckli 2007; Okogbue et al. 2009; Restrepo-Coupe et al., in preparation).

With the ever-increasing importance of the climate change debate, many eyes have turned towards the tropical zone as one of the critical 'driver' biomes of the world's climate system (Malhi and Wright 2004; IPCC 2007). Tropical forests play a major role in the dynamics of the global carbon and water cycles, storing more than half of all carbon found in terrestrial vegetation (Malhi et al. 2002a; IPCC 2007). Intact tropical forests in Amazonia and Africa have recently been providing a hugely significant 'ecosystem service' by increasing in biomass and absorbing ~12% of current anthropogenic CO_2 emissions (Lewis et al. 2009; Malhi 2010). They have been regulating the climate and cleaning the air we breathe and water we drink whilst also housing two thirds of the world's terrestrial biodiversity and providing the sustainable basis for life for millions of the world's poorest populations (Killeen 2007; Ghazoul and Sheil 2010). The prospect that these vast forests might soon be greatly reduced in extent (Zelazowski et al. 2011) makes it critical for us to understand their dynamics, how they do what they do for us, and how much and how quickly they might die back. Because of their vast extent, small changes in the radiation budget of tropical forests can have significant impacts on regional energy balances and, therefore, global carbon budgets, so questions such as these are a major focus of the climate change debate (IPCC 2007). Modelling canopy radiation, energy and carbon balances requires a vegetation model such as a dynamic global vegetation model (DGVM; Prentice et al. 2007; Zelazowski et al. 2011).

Models from the most recent generation of DGVMs incorporate high-detail representations of many ecosystem processes, which involve correspondingly heavy meteorological data requirements, especially when they are run at sub-daily time steps (Prentice et al. 2007; Landsberg and Sands 2011). L_d is a required input for most of these DGVMs, and some aspect of cloudiness (e.g. diffuse fraction of SW radiation, $f_{diffuse}$) is usually also necessary (Restrepo-Coupe et al., in preparation; e.g. Mercado et al. 2007 for the model *JULES*). Therefore, for practical reasons, tropical modellers can only apply DGVMs by making use of empirical or semi-empirical estimation schemes to 'fill the gaps' and generate values for variables such as L_d if they are unavailable (Muneer et al. 2004; e.g. Weishampel and Urban 1996 for the model *ZELIG*). There is a huge variety of estimation schemes for L_d—some of which have a long history and many have been encoded in 'weather generator' programs (e.g. Friend 1998; Ivanov et al. 2007) and 'pattern scaling' algorithms (Zelazowski et al. 2011). Almost all such schemes estimate L_d by estimating air emissivity, ε_a, first and then applying the Stefan–Boltzmann law (Brutsaert 1975; Prata 1996; Crawford and Duchon 1999; Niemelä et al. 2001; Iziomon et al. 2003; Flerchinger et al. 2009; Restrepo-Coupe et al., in preparation). Such 'gap filling' of missing meteorological data variables has recently become an important area of modelling in its own right (Falge et al. 2001; Stöckli 2007; Xing et al. 2008). Using such non-mechanistic rules, however, unavoidably introduces substantial uncertainty into the predictions of these models (stressed by Leigh 1999 for evapotranspiration and by Crawford and Duchon 1999 for energy balance calculations). Additionally, each scheme is based on a set of readings taken at a limited number of calibration sites, and it is at best optimistic that these should be globally applicable (even if claimed to be so, e.g. Swinbank 1963; Idso and Jackson 1969). The known large effect a change in gap filling/estimation scheme has within models on calculations of energy balance and, by extension, estimates of ecosystem productivity and carbon balance must be a cause for concern given the extreme importance of these quantities in the context of climate change (IPCC 2007). Few emissivity schemes for estimating L_d have been validated in tropical forests, so how much uncertainty is involved in using these schemes in the tropics?

In this study, we use a multiyear time series of hourly longwave data from the Caxiuanã station in Eastern Pará, Brazil, in order to compare several cloudiness estimation schemes. The data were collected as part of the Large-Scale Biosphere–Atmosphere Experiment in Amazonia (LBA; Avissar and Nobre 2002). The LBA flux tower at Caxiuanã

has been collecting high-quality measurements since 1999 (Carswell et al. 2002; Iwata et al. 2005), making it one of the best broad meteorological data sets available in the Amazon region. We apply 18 semi-empirical estimation rules to generate air emissivity, crossed with six sky cover estimation schemes, and validate all 18 × 6=108 combinations directly against measured values of L_d. In this way, we provide recommendations for best practice when gap filling longwave irradiance data at a tropical lowland site.

2 Methods

2.1 Site and instrumentation

The data used in this study are from the Caxiuanã LBA flux tower (eastern Pará state, Brazil, 1°43′11.26″ S, 51°27′ 29.45″ W) in the Estação Científica Ferreira Penna, maintained by the Museu Paraense Emílio Goeldi (Lisboa 1997; Malhi et al. 2009; Aragão et al. 2009), at 15 m a.s.l. in the lowland Amazon. This lowland tropical forest has a canopy height of 35 m, receives 2400-mm mean annual precipitation and has a mean annual temperature of 26.9°C (Iwata et al. 2005; Aragão et al. 2009). Air temperature and wind speed were measured at 53.0-m height (1.5-m above tower height), and the radiation sensor was a four-component CNR1 radiometer (Kipp & Zonen, Delft, the Netherlands) mounted lower down at 45.5 m to avoid solar panel reflection (Carswell et al. 2002; Iwata et al. 2005), so in this study, we took the reference height to be 53.0 m. Meteorological data were collected every hour during a 4.3-year period from 11 April 1999 to 12 August 2003, spanning 38,007 measurement hours (details in Iwata et al. 2005).

Tropical rainforests are far too diverse for any single site to be universally representative; however, the climate of Caxiuanã is typical of many lowland tropical forests not just in South America. Following the Köppen–Geiger classification system, the temperature, rainfall and seasonality regimes of Caxiuanã are very similar to the wetter lowland forests of Western Amazonia, the northern Guianas, the Caribbean coast of Central America, northern Democratic Republic of Congo and Southeast Asia between New Guinea and Mindanao (Peel et al. 2007).

2.2 Calculation of SW fluxes

The calculations used in this paper follow the methods fully described in standard textbooks (e.g. Iqbal 1983; Muneer et al. 2004; Şen 2008), so they are only summarised here. Conceptually, we proceed stepwise, starting with SW radiation received from the sun at the top of the atmosphere, then subtracting attenuation from clear sky turbidity to produce the 'clear sky' SW irradiance, then subtracting attenuation from clouds and aerosols to produce measured SW irradiance. Choosing to characterise cloudiness through sky cover and air emissivity (Table 1), we then used these quantities to estimate the clear sky emissivity, ε_{ac}, and also fractional sky cover due to clouds and aerosols, C (according to various schemes, Table 2 and Fig. 1). The effective emissivity under all conditions, ε_a, was then calculated from the SW fluxes, ε_{ac} and C (Table 3 and Table 4), leading finally to the downwelling LW flux, L_d.

SW downward radiation (insolation) received from sun and sky (i.e. direct + diffuse) on a horizontal detector surface (parallel to level ground below) placed just above the forest canopy (reference height), H_{TOC} (watts per square metre), was acquired from measurements at the Caxiuanã tower (Iwata et al. 2005). Theoretical SW radiation received on a horizontal surface placed at the top of the atmosphere, H_{TOA} (watts per square metre), was calculated at every time step (1 h) by the solar-positioning algorithm *SolPos* (Rymes 1998; translated into R, R Development Core Team 2011) using a solar constant of 1,367 W/m^2 (Iqbal 1983), from which the clearness index $K=H_{TOC}/H_{TOA}$ was also calculated (Table 1). SW radiation received on a horizontal surface at reference height specifically under a clear sky (meaning cloud-free and aerosol-free, but not free of clear sky scattering and absorption), H_{CLR} (watts per square metre, i.e. the value of H_{TOC} under perfectly clear conditions), was also necessary in order to divide clear sky SW radiation attenuation from the SW effects of clouds and aerosols (Perez et al. 1990; Konzelmann et al. 1994; Muneer et al. 2004), which have different dependencies over the diurnal cycle (e.g. in the Kasten model, clear sky SW turbidity depends only on pressure-corrected optical air mass, but SW cloud and aerosol effects depend on more factors; Muneer et al. 2004; n.b., these effects are also divided from the LW effects controlled by emissivity). H_{CLR} was summed from its direct and diffuse components, $H_{CLR,direct}$ and $H_{CLR,diffuse}$, which were calculated as follows. Firstly, the 'global model for the diffuse ratio' of Muneer et al. (2004)

$$f_{diffuse} = \begin{cases} 0.98 & \text{if } 0 \le K < 0.2 \\ 0.962 + 0.779K - 4.375K^2 + 2.716K^3 & \text{if } 0.2 \le K \le 1 \end{cases} \quad (1)$$

was rearranged by substituting $f_{diffuse} = \frac{H_{TOC,diffuse}}{H_{TOC}} = \frac{\tau_d}{\tau_D+\tau_d}$ and $K = \frac{H_{TOC}}{H_{TOA}} = \tau_D + \tau_d$ (where $\tau_D = H_{TOC,direct}/H_{TOA}$ and $\tau_d = H_{TOC,diffuse}/H_{TOA}$ are the transmission coefficients for direct and diffuse SW radiation, respectively; Liu and Jordan 1960), yielding an implicit equation which was then solved numerically to give $\tau_d = f(\tau_D)$. Specifically for clear skies, this may be written as:

$$\tau_{d,clearsky} = f\left(\tau_{D,clearsky}\right) \quad (2)$$

Table 1 Widely-used quantities and indices describing lack of clearness in the atmosphere. Note that these quantities in theory account not only for cloudiness effects (i.e. caused by visible suspended water droplets and ice crystals), but also the effects of Rayleigh (=molecular) scattering, atmospheric aerosols[a] (e.g. dust, smoke, pollution) and any radiation depletion caused by absorption or scattering by atmospheric water vapour and other trace gases (which can occur even under clear conditions; Muneer et al. 2004). Linke turbidity T_{LK} is not included because it is only considered in this text in the context of clear skies (Ineichen and Perez 2002; Muneer et al. 2004). We include SW and LW broadband indices only (and exclude spectral and PAR indices (Photosynthetically Active Radiation)). For a discussion of other indices, see 'sky clarity indices' and 'turbidity indices' in Muneer et al. (2004)

	Description	Notes
Sky cover, C	The fraction of the visible sky that is obscured or covered (i.e. fraction of completely overcast, 0–1)	Sometimes measured in tenths (e.g. Chang 1968; Doorenbos and Pruitt 1977) or oktas (=eighths, e.g. Doorenbos and Pruitt 1977; Kasten and Czeplak 1980; Muneer et al. 2004)[a]. Sky cover may be estimated from satellite data (e.g. ISCCP data; Rossow et al. 1985; Rossow and Schiffer 1991; http://isccp.giss.nasa.gov/index.html, as used by Butt et al. 2009).
Unclearness $(1 - K)$	K is the clearness index (0–1) of the atmosphere over shortwave wavelengths ($=H_{TOC}/H_{TOA}$, where H_{TOC} is the SW radiation received from sun and sky on a horizontal surface just above the forest canopy[b] (W/m^2) and H_{TOA} is the SW radiation that would theoretically be received from the sun on the same horizontal surface placed above the atmosphere (W/m^2). $(1 - K)$ is, therefore, a measure of atmospheric *un*clearness.	This definition follows Liu and Jordan (1960), Muneer et al. (2004) and many others. Note that in areas of steep topography or urban locations, skyline *shadowing* (the way a nearby building or mountain may reduce incoming radiation depending on the position of the solar disk; Dubayah and Rich 1995; Gabathuler et al. 2001) and *shading* (calculated from sky view factors; Dubayah and Rich 1995; Kanniah et al. 2010) must also be considered. Although often used for sub-daily data, we do not apply the correction of Perez et al. (1990) for removing the dependence of K on solar elevation because the K-dependent sky cover and emissivity schemes used here (Fig. 1 and Table 4) were derived for uncorrected K.
Overcast hours $(1 - (n/N))$	(n/N) is the relative sunshine duration (Martínez-Lozano et al. 1984; Spitters et al. 1986; Friend 1998), i.e. the fraction (0–1) of N=(maximum possible hours of sunshine) that is actually in bright sunshine, so $(1 - (n/N))$ is a measure of the duration of overcast periods.	Here, the word 'bright' means above approx. 210 W/m^2, which is the activation threshold for most sunshine recorders (Iqbal 1983). Usually used with monthly data where N=(average day length in hours) and n=(number of bright sunshine hours per day) and, unlike the other quantities considered here, cannot be used with meteorological data collected at a sub-daily time step, so will not be considered further.
Diffuse fraction, $f_{diffuse}$	Fraction (0–1) of downwelling SW radiation H_{TOC} received after having been scattered (and therefore not received from the solar disk directly but as 'sky light' or reflected light)[c] (Bindi et al. 1992; Muneer et al. 2004).	Note that even under clear skies, diffuse fraction should be nonzero because of the effects of CO_2 and other trace gases (Liu and Jordan 1960). If 'clear sky' effects are subtracted and aerosol effects are negligible, then $f_{diffuse}$ will coincide with the cloud-related diffuse radiation proportion (CRDRP) of Butt et al. (2009).
Effective air emissivity, ε_a	A fraction (0–1) defined by $\varepsilon_a = L_d/(\sigma\, T_c^4)$ (the Stefan–Boltzmann law where $\sigma = 5.67\times10^{-8}$ W m^{-2} K^{-4}, e.g. Monteith and Unsworth 1990), where L_d is the downward longwave radiation received at reference height above the forest canopy (in W/m^2, positive downwards) and T_c is the temperature of the transmitting object (in K).	The transmitting object is either the lowest cloud layer (under conditions of low cloud) or the lowest levels of the atmosphere (if cloudless or clouds are at high altitude with warmer air layers below; Kimball et al. 1982). Note that even under clear skies, air emissivity should be nonzero because of the effects of CO_2 and other trace gases (Prata 1996; Niemelä et al. 2001). Emissivity is strongly affected by cloud droplet size and microstructure (Lin et al. 2006), which is not accounted for by other cloudiness measures (e.g. sky cover).

Table 1 (continued)

	Description	Notes
Reflectance-based cloud indexes, n (satellite data)	In its simplest form, a cloud index is defined by $n=(\rho-\rho_{min})/(\rho_{max}-\rho_{min})$, where ρ is the reflectance as measured by satellite (Ineichen and Perez 1999). A cloud mask may be generated from these values through an appropriate thresholding algorithm (discussed in Kotarba 2010).	The ground reflectance (=ground albedo), ρ_{min}, and cloud reflectance, ρ_{max}, are values under clear and completely overcast conditions, as estimated from, e.g. 15-day means (Rossow et al. 1985). Reflectances may be recorded in several wavebands (not just at visible wavelengths), giving information on multiple cloud layers, e.g. MERIS data (http://envisat.esa.int/instruments/meris/) or the MODIS Cloud Mask product (http://modis-atmos.gsfc.nasa.gov/MOD35_L2/index.html; Lin et al. 2006; Kotarba 2010).
Cloud top height (satellite data)	Cloud top height is used in calculations of atmospheric radiative transfer (e.g. SBDART, http://arm.mrcsb.com/sbdart/) and is related to cloud thickness (e.g. Kanniah et al. 2010), but not directly to other aspects of cloudiness (e.g. emissivity is strongly affected by low-level clouds but much less by high-level cloud cover if the lower atmospheric levels remain clear).	Available from, e.g. GOES (http://www.goes-r.gov/products/ATBDs/cloud_height.pdf; Ellingson 1995; Ineichen and Perez 1999; Bisht and Bras 2010). Satellite observation data require interpolation to produce estimates across periods when images are obscured or unavailable (Wild 2008; Bisht and Bras 2010, e.g. when the source data are from a non-geostationary satellite making a regular overpass, for which only one or a few data points per day are possible), which requires independent knowledge of the cloudiness regime unavailable for this study.

[a] Despite being small solid or liquid particles that remain suspended in the air, cloud particles are not considered to be aerosols (Muneer et al. 2004)

[b] Doorenbos and Pruitt (1977) took 4 oktas to mean "50% of the sky covered all daytime hours by clouds or half of daytime hours the sky is fully clouded", but because we use sub-daily data, we can only accept the first of these

[c] H_{TOC} is also referred to as 'total' or 'global' radiation because it includes both direct and diffuse components (e.g. Liu and Jordan 1960), but we avoid this term because total radiation does not include incident LW radiation

[d] The term 'diffuse radiation' is used here to refer to short wavelength radiation coming from all parts of the sky except the solar disk (='indirect radiation' as opposed to 'beam irradiance' or 'direct radiation' received in a straight line from the solar disk; Liu and Jordan 1960; Ross 1975; Mercado et al. 2009). Atmospheric thermal radiation, L_d, although also diffuse in nature, is not included (Liu and Jordan 1960). Suits (1972) used 'diffuse' to refer to all light that had been intercepted and scattered by canopy components such as leaves, which is a widespread convention in forestry studies but unrelated to $f_{diffuse}$ here (this is referred to as 'complementary radiation' by Ross 1975). Note also that $f_{diffuse}$ is only approximately equal to the diffuse fraction of PAR radiation (as used in, e.g. Mercado et al. 2009) because atmospheric scattering differs between visible and infrared wavelengths ($f_{diffuse,PAR}$ is approximately $1.4 \times f_{diffuse,SW}$ under clear skies (Spitters et al. 1986; Friend 2001), decreasing to $1.0 \times f_{diffuse,SW}$ under overcast skies; Ross 1975; Monteith and Unsworth 1990)

Kasten's turbidity model (as presented in Ineichen and Perez 2002; Muneer et al. 2004) was then used to describe the hourly variation in clear sky radiation attenuation (predominantly due to scattering and absorption by air molecules and well-mixed gases, e.g. ozone, water vapour, but not aerosols or clouds), assuming a Linke turbidity of T_{LK}=2.74 (mean over the 0.11% of all points for which K> 0.76, indicating zero sky cover; Spitters et al. 1986) with no seasonal or inter-annual variation (cf. Muneer et al. 2004) to give:

$$\tau_{D,clearsky} = \exp(-\delta T_{LK} A) \quad (3)$$

where $\delta = \frac{1}{9.4+0.9A}$ (Perez et al. 1990; Ineichen and Perez 2002) and A is the pressure-corrected air mass (=(number of atmosphere depths between the sensor and the solar disk) × (above-canopy pressure)/(sea level pressure); Rymes 1998). The value $\tau_{D,clearsky}$ from Eq. 3 was then used to calculate $\tau_{d,clearsky}$ using Eq. 2 and then H_{CLR} using:

$$H_{CLR} = H_{CLR,direct} + H_{CLR,diffuse} = \left(\tau_{D,clearsky} + \tau_{d,clearsky}\right) H_{TOA} \quad (4)$$

Calculation of H_{CLR} is necessary because it is used in several sky cover schemes (Table 3 and Fig. 1) and the emissivity schemes based on them (Table 4). Note that the ratios H_{CLR}/H_{TOA} (which quantifies clear sky effects independent of sky cover, e.g. Flerchinger et al. 2009) and H_{TOC}/H_{CLR} (which quantifies the effects of clouds and aerosols, e.g. Kasten and Czeplak 1980; Crawford and Duchon 1999; Jegede et al. 2006; Lhomme et al. 2007; Stöckli 2007; called 'relative shortwave radiation' in Allen et al. 1998 and 'solar index' in Flerchinger et al. 2009) are also referred to as

Table 2 Estimation schemes for clear-sky[a] air emissivity (i.e. all these schemes were derived from data on cloud-free, aerosol-free days only) T_a is air temperature (K) and e is ambient vapour pressure (mb or hPa), both measured at reference height (=53 m at Caxiuanã), w is the precipitable water in the air column (mm or kg/m^2) calculated as $w=465e/T_a$ (Prata 1996), and T_c is the temperature of the cloud base (K) estimated by the ambient dew point temperature[b]. Because the Caxiuanã site is only slightly above sea level, no elevation correction was applied to these schemes (q.v. Flerchinger et al. 2009). All emissivity estimates were constrained to be between 0 and 1. Note that, although these schemes assume clear-sky conditions, the effects of factors unrelated to sky cover (e.g. clear sky turbidity) on downwelling LW flux may still contribute (e.g. even at low water vapour content, Prata's scheme predicts nonzero ε_{ac} partly due to CO_2 effects; Prata 1996). Note also that saturated vapour pressure does not vary independently of T_a (see, e.g. the Goff–Gratch equation; Hellwege and Madelung 1988) and therefore at constant humidity neither does e, which must be taken into account when assessing whether or not emissivity increases or decreases with T_a

Scheme	ε (constrained so that $0\leq\varepsilon\leq1$)	Code	Notes
Ångström (1915)	$\varepsilon = 0.83 - 0.18*\left(10^{-0.067e}\right)$	CAN	The Ångström formulation was originally quoted with variable constants to be fitted on a site-by-site basis, viz. $\varepsilon=\alpha-\beta(10^{-\gamma e})$. Also used by Anderson (1954) and Iziomon et al. (2003), and the values here are for summer data from Sodankylä (Finland; Niemelä et al. 2001; also used by Flerchinger et al. 2009).
Brunt (1932)[c]	$\varepsilon = 0.51 + 0.066\sqrt{e}$	CBR	The Brunt equation was originally quoted with variable constants, viz. $\varepsilon=a+b\sqrt{e}$. Also used by Penman (1948), Anderson (1954), Brutsaert (1975, 1982), Niemelä et al. (2001), Iziomon et al. (2003), Flerchinger et al. (2009) and the values here are as recommended in Brutsaert (1975) as a "satisfactory mean curve through data by several other authors".
Swinbank (1963)	$\varepsilon = 0.0000092{T_a}^2$	CSW	Based on data from Aspendale (VIC, Australia), Kerang (VIC, Australia), the Indian Ocean and Benson (UK). Also used by Idso (1981), Brutsaert (1982), Prata (1996), Dilley and O'Brien (1998), Crawford and Duchon (1999), Pirazzini et al. (2000), Niemelä et al. (2001), Iziomon et al. (2003), Flerchinger et al. (2009)
Idso and Jackson (1969)	$\varepsilon = 1 - 0.261\exp\left(-0.000777(273 - T_a)^2\right)$	CIJ	Based on data from Point Barrow (AK, USA), Phoenix (AZ, USA), Aspendale (VIC, Australia), Kerang (VIC, Australia) and the Indian Ocean. Also used by Idso (1981), Brutsaert (1982), Prata (1996), Crawford and Duchon (1999), Pirazzini et al. (2000), Iziomon et al. (2003), Flerchinger et al. (2009)
Brutsaert (1975, 1982)	$\varepsilon = 1.24\left(\frac{e}{T_a}\right)^{\frac{1}{7}}$	CBT	Based on data from "several other authors". Also used by Idso (1981), Campbell (1985), Prata (1996), Campbell and Norman (1998), Crawford and Duchon (1999), Pirazzini et al. (2000), Niemelä et al. (2001), Iziomon et al. (2003), Lhomme et al. (2007), Flerchinger et al. (2009), Restrepo-Coupe et al., in preparation
Idso (1981)	$\varepsilon = 0.7 + 0.0000595e \times \exp\left(\frac{1500}{T_a}\right)$	CID	Based on data from Phoenix (AZ, USA). Also used by Kimball et al. (1982), Prata (1996), Pirazzini et al. (2000), Niemelä et al. (2001), Flerchinger et al. (2009), Restrepo-Coupe et al., in preparation
Monteith and Unsworth (1990)	$\varepsilon = \frac{1}{\sigma{T_c}^4}\left(-119 + 1.06\sigma{T_a}^4\right)$	CMU	Based on data from the English Midlands

Table 2 (continued)

Scheme	ε (constrained so that $0 \le \varepsilon \le 1$)	Code	Notes
			(UK).
Konzelmann et al. (1994)	$\varepsilon = 0.23 + 0.484\left(\frac{e}{T_a}\right)^{\frac{1}{8}}$	CKZ	Based on data from Greenland (Denmark). Also used by Pirazzini et al. (2000).
Prata (1996)	$\varepsilon = 1 - \left(\left(1+\frac{w}{10}\right)\exp\left(-\sqrt{1.2+3\times\frac{w}{10}}\right)\right)$	CPR	Based on a worldwide data set. Also used by Pirazzini et al. (2000), Niemelä et al. (2001), Lhomme et al. (2007), Flerchinger et al. (2009). This scheme is currently in general use for analysing MODIS data (e.g. Bisht and Bras 2010)
Dilley and O'Brien (1998), model B	$\varepsilon = \frac{1}{\sigma T_c^4}\left(59.38 + \left(113.7\times\left(\frac{T_a}{273.16}\right)^6\right) + \left(96.96\sqrt{\frac{w}{25}}\right)\right)$	CDO	Based on a worldwide data set. Also used by Niemelä et al. (2001), Lhomme et al. (2007), Flerchinger et al. (2009), Restrepo-Coupe et al., in preparation

[a] Some sources use the term 'clear sky' to refer to cloud-free conditions and 'pristine sky' to cloud-free and aerosol-free conditions (e.g. Crawford and Duchon 1999; Rose et al. 2006). We, however, follow the more common usage of 'clear sky' to mean both cloud- and aerosol-free (though not free of radiation depletion by factors unrelated to sky cover such as absorption by permanent trace gases and water vapour; Prata 1996; Niemelä et al. 2001; Muneer et al. 2004) mainly because interactions between aerosol concentration and cloud cover mean that they do not act independently in general (Lin et al. 2006; Mercado et al. 2009; Kanniah et al. 2010). This is in keeping with widely used terminology such as 'clear air turbulence' as used in the aviation industry. However, we note that all of the all-sky estimation schemes considered in this text, except those of the LBA-MIP and Lhomme, are explicitly dependent on sky cover only (Table 4) and therefore account for overcast conditions under the implicit assumption that aerosol contamination and cloud contamination are equal at least in terms of calculated emissivity (i.e. 1 okta of cloud is the same as 1 okta of pollution, smoke from large-scale fires or dust load), which is only approximately true. Emissivity schemes which consider atmospheric aerosols separately from cloud cover are beyond the scope of this study (see, e.g. Crawford and Duchon 1999; Kanniah et al. 2010)

[b] As explained in Kimball et al. (1982) and Niemelä et al. (2001), the temperature here should be that of the emitting object, which is usually, but not always, the visible cloud base. Especially when the cloud base is at high altitude, the lowest atmospheric layers closest to the canopy (which may be transparent at visible wavelengths but not at infrared) can be warmer than the cloud base and therefore will make a greater contribution to LW radiation received at the surface. Estimating the 'cloud base' temperature from the dew point allows a bias towards warmer temperatures that may be assumed to correct for such conditions

[c] As originally presented, the Brunt equation was used to calculate air emissivity for downward longwave flux (Brunt 1932), and we follow this practice (as did Anderson 1954; Brutsaert 1975; Niemelä et al. 2001; Flerchinger et al. 2009), even though we note that the same equation is also often used (with different parameter values) to calculate net upward longwave flux (e.g. Chang 1968; Dunne and Leopold 1978; Leigh 1999; and the recommended FAO method for calculating net radiation, Allen et al. 1998) or both upward and downward fluxes (e.g. Penman 1948)

clearness indices by some sources (Martínez-Lozano et al. 1984; Gabathuler et al. 2001), but we reserve that term exclusively for the most commonly used clearness index K as defined above (which quantifies all atmospheric radiation depletion, e.g. Liu and Jordan 1960; Spitters et al. 1986; Perez et al. 1990; Weishampel and Urban 1996; Muneer et al. 2004; Okogbue et al. 2009). In order to constrain these ratios to the interval 0–1, we ensured that $H_{TOA} > H_{CLR}$, $H_{CLR} > H_{TOC}$ and $H_{TOA} > H_{TOC}$ at all time points.

An environmental lapse rate of 0.0060°C/m was assumed with no seasonal or inter-annual variation (Mokhov and Akperov 2006; it was also assumed that inverted conditions did not occur, cf. Walsh 1996; Niemelä et al. 2001), and the modified barometric formula for a vertical temperature gradient (Berberan-Santos et al. 1997; differing from the standard barometric formula, e.g. Stöckli 2007) was used to calculate ambient pressure from an assumed sea level pressure of 1,013.25 hPa when measured pressure was unavailable. Saturated vapour pressure was calculated using the Goff–Gratch equation ('Landolt–Börnstein' form; Hellwege and Madelung 1988).

2.3 Calculation of emissivity and LW fluxes

'Cloudiness' is a term that has been used to refer to several distinct meteorological quantities (Table 1). Although in general these measures correlate with each other (e.g. as a general rule, when sky cover is high SW diffuse fraction is also high), when considering sub-daily data (as in this study) and comparing with other studies using a variety of different measures, the differences between cloudiness quantities become important. For example, if cloud cover is persistent and uniform but consists sometimes of thin, high-altitude stratiform clouds and sometimes of warmer, low-level cumuliform clouds, then sky cover, unclearness, cloud index, overcast hours and probably diffuse fraction will all remain approximately constant, but air emissivity, cloud top height, cloud thickness and opacity could vary greatly (Niemelä et al. 2001; Kotarba 2010).

Several estimates of sky cover fraction are available based on either $K = H_{TOC}/H_{TOA}$ or (H_{TOC}/H_{CLR}) and could be calculated for each time step (Fig. 1). Diffuse fraction, $f_{diffuse}$, is also routinely estimated by a variety of formulae

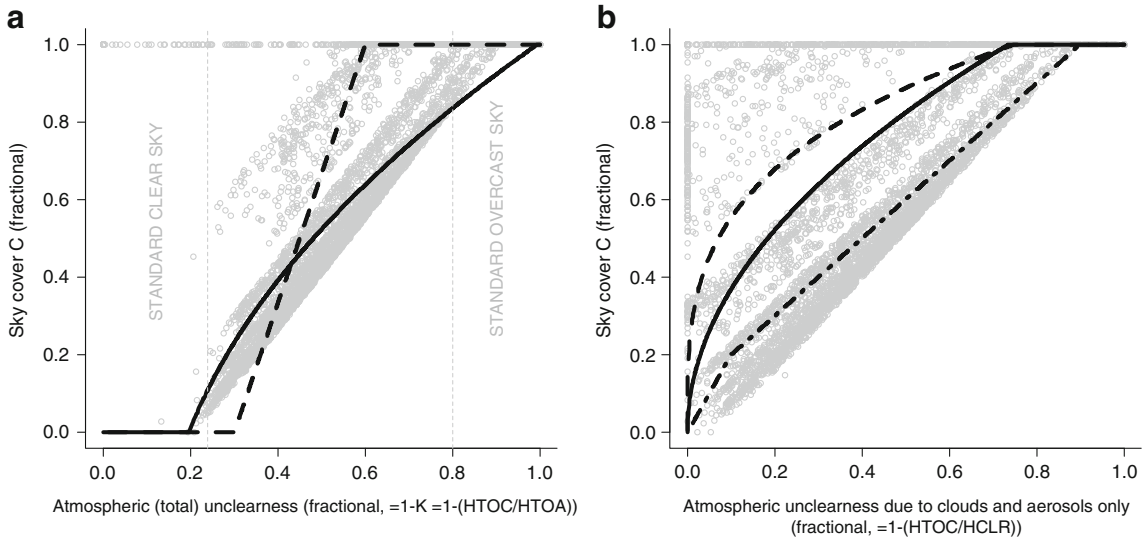

Fig. 1 Estimates of sky cover fraction (C) as functions of atmospheric clearness (see Table 3 for equations): the quadratic regression of Black (*solid line* in **a**); the linear regression of Campbell (*broken line* in **a**); and the schemes of Weishampel and Urban (*grey points* in **a**, **b**), Kasten and Czeplak (*dashed line* in **b**), Konzelmann et al. (*solid line* in **b**) and Jegede et al. (*dash-dot line* in **b**). For reference, *vertical broken lines* in **a** indicate the standard clear and overcast skies suggested by Spitters et al. (1986), where C should be minimal and maximal (respectively) for all schemes; however, these thresholds were intended for daily data (the points plotted here are hourly), and other authors have used different clearness thresholds (e.g. Iqbal 1983; Okogbue et al. 2009, and, of course, the equations illustrated here)

(Goudriaan 1977; Kasten and Czeplak 1980; Iqbal 1983; Weishampel and Urban 1996; Friend 2001; reviewed in Spitters et al. 1986; Bindi et al. 1992; Muneer et al. 2004; Şen 2008), and there are 'Ångström formula'-style relationships for estimating cloudy hours (Ångström 1924; Penman 1948; Black 1956; Chang 1968; Doorenbos and Pruitt 1977; Dunne and Leopold 1978; Brutsaert 1982; Iqbal 1983; Allen et al. 1998; reviewed in Martínez-Lozano et al. 1984; Spitters et al. 1986; Muneer et al. 2004; Landsberg and Sands 2011), but we did not have independent measurements of diffuse fraction or cloudy hours in this study and therefore could not use them for validation purposes.

Estimation schemes for emissivity may be divided into 'clear sky' schemes which assume a cloudless, aerosol-free atmosphere (Table 2) and 'all-sky' schemes intended to be applicable under all conditions (Table 4). All-sky emissivity schemes attempt to incorporate the effects of clouds and aerosols, which is essential in order for these schemes to be useable in most parts of the world (including Caxiuanã). The general (though not universal) approach is to combine one of the clear sky emissivity schemes with one of the accepted cloud cover estimation functions (Table 3, Fig. 1), and this has been done in a large variety of ways (see reviews by Prata 1996; Dilley and O'Brien 1998; Crawford and Duchon 1999; Gabathuler et al. 2001; Niemelä et al. 2001; Flerchinger et al. 2009). In this paper, we have selected and implemented 18 of the most widely used of these clear-sky and all-sky schemes, and through the use of the Stefan–Boltzmann law (Table 1), each time series of estimated air emissivities was converted into estimated longwave down (L_d) values (although not all schemes were derived from tropical or worldwide data sets (Tables 2 and 3), they are intended as general use relationships, so we considered them all to be potentially applicable at Caxiuanã).

2.4 Model testing and evaluation

The period 1 April 2002 to 31 July 2003 was selected to be used for the comparison of L_d estimation schemes because above-canopy pressure was only available during this period and sensor breaks for other ambient variables were minimal. The optimal estimation scheme was then applied to the remaining data points, yielding a comparison between these estimated L_d values and the true L_d values measured directly at the Caxiuanã tower. The goodness of fit for all estimation schemes was assessed using root mean squared (RMS) errors summed over all available data points (Flerchinger et al. 2009).

3 Results

The difference between the observed and expected longwave downward flux L_d was assessed by RMS errors (Table 5), applying an arbitrary threshold of 20 W/m^2 RMS error below which the scheme was considered acceptable for use (corresponding to emissivity values within approx. 0.0423 of observed; n.b., Iziomon et al. 2003 required

Table 3 Estimation schemes for sky cover fraction (C, all estimates were constrained to be between 0 and 1). Note that these sky cover schemes are all either functions of $K=H_{TOC}/H_{TOA}$ or (H_{TOC}/H_{CLR}), except that of Weishampel and Urban (1996) which is a function of H_{TOC} and H_{TOA} separately

Scheme	C (constrained so that $0 \le C \le 1$)	Notes
Quadratic regression of Black (1956)	$C = \frac{0.34-\sqrt{0.34^2+4\times0.458\times(0.803-K)}}{-2\times0.458}$	Based on a worldwide data set. Formerly very widely used (e.g. Chang 1968; Dunne and Leopold 1978; Gates 1980; Iqbal 1983)
Kasten and Czeplak (1980)	$C = \left(\frac{4}{3}\left(1-\frac{H_{TOC}}{H_{CLR}}\right)\right)^{\frac{1}{3.4}}$	Based on data from Hamburg, Germany
Campbell (1985)	$C = 2.33 - 3.33K$	Recommended by Flerchinger et al. (2009)
Konzelmann et al. (1994)	$C = \sqrt{\frac{1}{0.78\times\exp(-0.00085\times(\text{altitude in metres}))}\left(1-\frac{H_{TOC}}{H_{CLR}}\right)}$	Based on data from Greenland, Denmark. The equation used in *WeatherG* is the special case of this for a site at altitude 214.5 m a.s.l. (Ivanov et al. 2007).
Weishampel and Urban (1996)	$C = 1 + \frac{252.7-(H_{TOC}\times60\times60\times24/(4.19\times10{,}000))}{0.695(H_{TOA}\times60\times60\times24/(4.19\times10{,}000))}$	Based on data from Belize City, Belize. As used in the model *ZELIG*
Jegede et al. (2006)	$C = \begin{cases} 1.1-\frac{H_{TOC}}{H_{CLR}} & 0 \le \frac{H_{TOC}}{H_{CLR}} < 0.9 \\ 2\left(1-\frac{H_{TOC}}{H_{CLR}}\right) & 0.9 \le \frac{H_{TOC}}{H_{CLR}} \le 1 \end{cases}$	Based on data from Ile-Ife, Nigeria

errors below ±5 W/m^2 in Germany, but it appears either that variability at this tropical location is inherently higher than in Germany or that uncertainties in these estimation schemes are still higher than desirable; Monteith and Unsworth 1990 accepted errors of the order ±30 W/m^2 for L_d, which corresponds approximately to the 6% specified by Konzelmann et al. 1994; Ellingson 1995 indicated that ±10 W/m^2 was desirable for oceanic surface radiation budgets but, because this was seldom achieved, considered data with reported errors up to ±50 W/m^2). An acceptable scheme would be one where the L_d values match closely both in terms of mean and variance; however, we found that even the most closely matching schemes did not match well in variance terms (Fig. 2), so we used seasonal and diurnal/nocturnal means to assess relative performance. We considered both 'clear sky' and 'all-sky' estimation schemes even when sky cover was nonzero (cf. Flerchinger et al. 2009) because we found that some clear sky schemes consistently performed very well under all conditions.

We considered sunny daylight hours first because from a vegetation modelling perspective, these are the most critical points at which to have the canopy energy balance correct (these are points at which photosynthesis will be maximal and therefore contribute most strongly to overall productivity calculations; Mercado et al. 2009; 'sunny' was defined by $H_{TOC}>750$ W/m^2; Gates 1980: At Caxiuanã, this was a slightly less restrictive condition than requiring clear skies with $K>0.76$; Spitters et al. 1986). RMS errors showed that during sunny daylight hours at Caxiuanã, the schemes which predicted L_d (equivalently, effective air emissivity) most correctly in the dry season were ε_{CSW}, ε_{CIJ} and ε_{CDO} (all independent of sky cover scheme; please see Tables 2 and 4 for subscript codes); ε_{AAN} (using Black, Campbell, Weishampel–Urban or Jegede only, but best with Weishampel–Urban); ε_{AMU} (using Black, Campbell, Weishampel–Urban or Jegede, but best with Jegede); ε_{AGB} (using Black, Campbell, Weishampel–Urban or Jegede, best with Weishampel–Urban); and ε_{ADK} (using any sky cover scheme, but best with Konzelmann). Considering each scheme over all daylight hours (not just sunny hours) at Caxiuanã, RMS errors showed that during the dry season, ε_{CIJ} and ε_{CDO} (both independent of sky cover scheme), ε_{AMU} (using Jegede only), and ε_{ADK} (using any sky cover scheme, best with Weishampel–Urban) estimated L_d within the 20-W/m^2 threshold.

We also considered the performance of each scheme over nocturnal hours at Caxiuanã. Several emissivity schemes cannot be evaluated during the night, so gap filling of nighttime values is advised using either an average of the previous afternoon's values (e.g. Lhomme et al. 2007) or interpolation using a regression on general daylight values (e.g. Stöckli 2007) or more complex algorithms including nonlinear techniques (Falge et al. 2001; Xing et al. 2008), but we conservatively did not gap-fill the nighttime values here in order to remove uncertainty related to temporal gap filling in the comparison. Other schemes were originally designed for daily average values (e.g. the Brunt equation) and therefore prescribe no specific treatment of nocturnal hours, but we follow general practice and apply them as if designed for

Table 4 Estimation schemes for effective air emissivity ε_a. T_a is air temperature (Kelvin), *RH* is relative humidity (per cent) and *e* is ambient vapour pressure (millibars or hectopascals), all measured at reference height (=53 m at Caxiuanã); *C* is sky cover fraction and T_c is the temperature of the cloud base (Kelvin) estimated by the ambient dew point temperature. Because the Caxiuanã site is only slightly above sea level, no elevation correction was applied to these schemes (q.v. Flerchinger et al. 2009). All emissivity estimates were constrained to be between 0 and 1. Note that most schemes are dependent on *C* and therefore vary depending on which estimation equation for this is applied (q.v. Table 3 and Fig. 1). The LBA-MIP scheme as described in Stöckli (2007) required nighttime values to be replaced by a linear interpolation based on a regression applied to daylight values, and that of Lhomme et al. (2007) required nocturnal values to be estimated as equal to afternoon conditions on the previous day; however, we have not applied these or any other temporal gap-filling schemes (nocturnal values for both these schemes were left undefined)

Scheme	ε (constrained so that $0 \le \varepsilon \le 1$)	Code	Notes
Ångström (1915)	$\varepsilon = \varepsilon_{CAN}(1 + 0.22C)$	AAN	Where ε_{CAN} is the ε of the Ångström scheme (Table 2). The extra $(1+(0.22 \times C))$ accounts for sky cover following Brutsaert's (1982) method (see Flerchinger et al. 2009).
Brutsaert (1982)'s version of the Brunt equation	$\varepsilon = \varepsilon_{CBR}(1 + 0.22C)$	ABR	Where ε_{CBR} is the ε of the Brunt scheme (Table 2). The extra $(1+(0.22 \times C))$ accounts for sky cover following Brutsaert's (1982) method (see Flerchinger et al. 2009).
Monteith and Unsworth (1990)	$\varepsilon = \left(1 - \left(1 - \frac{4(T_a - T_c)}{T_a}\right)C\right)\varepsilon_{CMU} + \left(1 - \frac{4(T_a - T_c)}{T_a}\right)C$	AMU	where ε_{CMU} is the ε of the Monteith and Unsworth scheme (Table 2). Based on data from Oxford (UK). A special case of this with $1 - \frac{4(T_a - T_c)}{T_a} = 0.84$ appears in Campbell (1985) and Flerchinger et al. (2009).
HYBRID (Friend et al. 1997, 2009)	$\varepsilon = 0.69(1 - C^6) + 0.979C^4$	AHY	Developed from Konzelmann et al. (1994) and Pirazzini et al. (2000), with this form being that used in the model *HYBRID* (Friend et al. 1997, 2009).
Gabathuler et al. (2001)	$\varepsilon = \left(\frac{0.84(RH-68)}{\sigma T_a^4} + \left(1 - \frac{21}{T_a}\left(\frac{H_{TOC}}{H_{CLR}}\right)\right)^4\right)(1 + 0.22C^2)$	AGB	Based on data from stations in Switzerland.
LBA-MIP (Stöckli 2007)	$\varepsilon = \varepsilon_{CID}\left(1 + 0.3\left(1 - \frac{H_{TOC}}{H_{CLR}}\right)^2\right)$	ALM	Where ε_{CID} is the ε of the Idso scheme (Table 2); however, nighttime *K* values have not been linearly interpolated as in Stöckli (2007). Developed from Idso (1981) and Gabathuler et al. (2001). This scheme is the currently accepted protocol of the LBA-MIP project (Avissar and Nobre 2002; http://www.climatemodeling.org/lba-mip/).
Lhomme et al. (2007)	$\varepsilon = \left(\frac{1.18}{1.24}\varepsilon_{CBT}\right)\left(-0.34\frac{H_{TOC}}{H_{CLR}} + 1.37\right)$	ALH	Where ε_{CBT} is the ε of the Brutsaert scheme (Table 2); however, nighttime *K* values were not replaced by the mean value of *K* calculated the previous day between 1400 and 1630 hours, as in Lhomme et al. (2007). Based on data from Condoriri (Bolivia).
Dilley–Kimball scheme from Flerchinger et al. (2009)	$\varepsilon = \varepsilon_{CDO} + (1 - \varepsilon_{8z}(1.4 - 0.4\varepsilon_{8z}))Cf_{8i}$	ADK	Where ε_{CDO} is the ε of the Dilley and O'Brien model B scheme (Table 2), $\varepsilon_{8z} = 0.24 + \left(0.00000298\left(\frac{e}{10}\right)^2 \exp\left(\frac{3{,}000}{T_a}\right)\right)$ is the sky emissivity in the zenith direction and $f_{8i} = -0.6732 + 0.00624T_c - 0.00000914T_c^2$ (Kimball et al. 1982). Based on data from Sidney (MT, USA), Phoenix, AZ, USA (Kimball et al. 1982) combined with a worldwide data set (Dilley and O'Brien 1998). Also used by Restrepo-Coupe et al., in preparation

use at all sub-daily time points (e.g. Prata 1996; Flerchinger et al. 2009). During the dry season, ε_{CAN}, ε_{CBR}, ε_{CIJ} and ε_{CDO} (all independent of sky cover scheme) performed well (with ε_{CDO} marginally the best).

We consider the wet season at Caxiuanã separately from the dry season. During sunny daylight hours in the wet season, ε_{CAN}, ε_{CSW} and ε_{CIJ} (all independent of sky cover scheme); ε_{AAN} (using Black, Campbell, Weishampel–Urban

Table 5 RMS errors summed over all available data points (all in watts per square metre) for each estimation scheme for longwave downward radiation received at the top of the canopy (columns; headings are the corresponding emissivity schemes; for codes, see Tables 2 and 4) combined with each sky cover scheme (rows; see Table 3 and Fig. 1). Errors for the recommended schemes ADK and CDO are in bold. Note that nocturnal values for the all-sky schemes cannot be calculated (see Table 4)

	ε_{CAN}	ε_{CBR}	ε_{CSW}	ε_{CIJ}	ε_{CBT}	ε_{CID}	ε_{CMU}	ε_{CKZ}	ε_{CPR}	$\boldsymbol{\varepsilon_{CDO}}$	ε_{AAN}	ε_{ABR}	ε_{AMU}	ε_{AHY}	ε_{AGB}	ε_{ALM}	ε_{ALH}	ε_{ADK}
During sunny daylight hours in the dry season																		
Black	21.57	26.52	16.79	9.01	27.30	60.80	28.53	125.93	21.33	12.29	11.30	55.11	7.87	79.56	10.81	60.80	51.02	**9.25**
Kasten–Czeplak	21.57	26.52	16.79	9.01	27.30	60.80	28.53	125.93	21.33	12.29	41.13	60.78	34.70	20.36	39.41	60.80	51.02	**9.23**
Campbell	21.57	26.52	16.79	9.01	27.30	60.80	28.53	125.93	21.33	12.29	10.51	46.83	13.48	82.62	11.17	60.80	51.02	**10.55**
Konzelmann	21.57	26.52	16.79	9.01	27.30	60.80	28.53	125.93	21.33	12.29	29.11	60.32	22.78	49.86	25.04	60.80	51.02	**8.78**
Weishampel–Urban	21.57	26.52	16.79	9.01	27.30	60.80	28.53	125.93	21.33	12.29	7.15	46.96	10.89	84.55	9.54	60.80	51.02	**10.03**
Jegede	21.57	26.52	16.79	9.01	27.30	60.80	28.53	125.93	21.33	12.29	11.41	55.58	7.81	79.67	10.54	60.80	51.02	**9.14**
During sunny daylight hours in the wet season																		
Black	16.75	35.31	14.63	13.89	36.13	69.41	23.35	117.99	30.29	21.09	14.58	57.91	11.07	74.91	10.86	69.42	51.07	**18.15**
Kasten–Czeplak	16.75	35.31	14.63	13.89	36.13	69.41	23.35	117.99	30.29	21.09	44.49	69.35	38.00	25.99	33.99	69.42	51.07	**13.97**
Campbell	16.75	35.31	14.63	13.89	36.13	69.41	23.35	117.99	30.29	21.09	11.26	44.10	15.52	77.19	11.01	69.42	51.07	**20.42**
Konzelmann	16.75	35.31	14.63	13.89	36.13	69.41	23.35	117.99	30.29	21.09	31.08	68.30	24.68	54.99	20.27	69.42	51.07	**15.68**
Weishampel–Urban	16.75	35.31	14.63	13.89	36.13	69.41	23.35	117.99	30.29	21.09	10.70	49.74	12.03	77.52	10.50	69.42	51.07	**19.17**
Jegede	16.75	35.31	14.63	13.89	36.13	69.41	23.35	117.99	30.29	21.09	15.33	59.33	11.23	74.74	10.60	69.42	51.07	**17.87**
During daylight hours in the dry season																		
Black	21.27	25.56	20.69	14.33	26.67	59.56	30.47	123.81	21.67	14.79	31.55	57.95	25.44	51.95	37.22	61.51	52.23	**11.52**
Kasten–Czeplak	21.27	25.56	20.69	14.33	26.67	59.56	30.47	123.81	21.67	14.79	46.87	58.75	41.49	35.43	49.98	61.51	52.23	**12.25**
Campbell	21.27	25.56	20.69	14.33	26.67	59.56	30.47	123.81	21.67	14.79	45.49	57.67	42.22	51.22	47.12	61.51	52.23	**12.25**
Konzelmann	21.27	25.56	20.69	14.33	26.67	59.56	30.47	123.81	21.67	14.79	38.87	57.05	33.76	39.93	44.46	61.51	52.23	**12.18**
Weishampel–Urban	21.27	25.56	20.69	14.33	26.67	59.56	30.47	123.81	21.67	14.79	37.37	58.18	34.23	61.50	41.46	61.51	52.23	**11.48**
Jegede	21.27	25.56	20.69	14.33	26.67	59.56	30.47	123.81	21.67	14.79	22.61	53.00	19.25	63.85	32.56	61.51	52.23	**12.34**
During daylight hours in the wet season																		
Black	25.29	28.84	27.74	22.53	29.11	59.74	35.95	125.12	25.20	21.09	31.73	57.53	26.29	49.81	37.27	62.69	51.26	**17.03**
Kasten–Czeplak	25.29	28.84	27.74	22.53	29.11	59.74	35.95	125.12	25.20	21.09	46.49	58.36	42.25	38.97	47.11	62.69	51.26	**16.44**
Campbell	25.29	28.84	27.74	22.53	29.11	59.74	35.95	125.12	25.20	21.09	41.27	55.00	39.37	51.75	41.66	62.69	51.26	**17.61**
Konzelmann	25.29	28.84	27.74	22.53	29.11	59.74	35.95	125.12	25.20	21.09	39.81	57.30	35.82	43.61	42.50	62.69	51.26	**17.04**
Weishampel–Urban	25.29	28.84	27.74	22.53	29.11	59.74	35.95	125.12	25.20	21.09	37.72	57.60	34.35	54.55	39.97	62.69	51.26	**16.59**
Jegede	25.29	28.84	27.74	22.53	29.11	59.74	35.95	125.12	25.20	21.09	26.53	53.27	23.39	58.88	35.42	62.69	51.26	**18.05**
During nighttime hours in the dry season																		
Black	15.79	19.70	20.49	14.96	24.94	59.76	28.31	115.23	21.64	14.94	–	–	–	–	–	–	–	–
Kasten–Czeplak	15.79	19.70	20.49	14.96	24.94	59.76	28.31	115.23	21.64	14.94	–	–	–	–	–	–	–	–
Campbell	15.79	19.70	20.49	14.96	24.94	59.76	28.31	115.23	21.64	14.94	–	–	–	–	–	–	–	–
Konzelmann	15.79	19.70	20.49	14.96	24.94	59.76	28.31	115.23	21.64	14.94	–	–	–	–	–	–	–	–

Table 5 (continued)

	ε_{CAN}	ε_{CBR}	ε_{CSW}	ε_{CJI}	ε_{CBT}	ε_{CID}	ε_{CMU}	ε_{CKZ}	ε_{CPR}	ε_{CDO}	ε_{AAN}	ε_{ABR}	ε_{AMU}	ε_{AHY}	ε_{AGB}	ε_{ALM}	ε_{ALH}	ε_{ADK}
Weishampel–Urban	15.79	19.70	20.49	14.96	24.94	59.76	28.31	115.23	21.64	14.94	–	–	–	–	–	–	–	–
Jegede	15.79	19.70	20.49	14.96	24.94	59.76	28.31	115.23	21.64	14.94	–	–	–	–	–	–	–	–
During nighttime hours in the wet season																		
Black	27.69	19.95	33.75	26.45	19.63	47.98	41.94	127.71	18.26	19.37	–	–	–	–	–	–	–	–
Kasten–Czeplak	27.69	19.95	33.75	26.45	19.63	47.98	41.94	127.71	18.26	19.37	–	–	–	–	–	–	–	–
Campbell	27.69	19.95	33.75	26.45	19.63	47.98	41.94	127.71	18.26	19.37	–	–	–	–	–	–	–	–
Konzelmann	27.69	19.95	33.75	26.45	19.63	47.98	41.94	127.71	18.26	19.37	–	–	–	–	–	–	–	–
Weishampel–Urban	27.69	19.95	33.75	26.45	19.63	47.98	41.94	127.71	18.26	19.37	–	–	–	–	–	–	–	–
Jegede	27.69	19.95	33.75	26.45	19.63	47.98	41.94	127.71	18.26	19.37	–	–	–	–	–	–	–	–

or Jegede, best with Weishampel–Urban); ε_{AMU} (using Black, Campbell, Weishampel–Urban or Jegede, best with Black); ε_{AGB} (using Black, Campbell, Weishampel–Urban or Jegede, best with Weishampel–Urban); and ε_{ADK} (using Black, Kasten–Czeplak, Konzelmann, Weishampel–Urban or Jegede, best with Kasten–Czeplak) all predicted L_d acceptably well (Table 5 and Fig. 2a, b). During all daylight hours in the wet season, only ε_{ADK} (under any sky cover scheme, marginally best with Kasten–Czeplak) achieved the 20-W/m^2 threshold (Table 5 and Fig. 2c, d). Finally, during nocturnal hours in the wet season, ε_{CBR}, ε_{CBT}, ε_{CPR} and ε_{CDO} (all independent of sky cover scheme) gave good estimates (with ε_{CPR} the best; Table 5 and Fig. 2e, f).

Based on these results, our recommended schemes for estimating longwave downward flux at this tropical lowland site are the Dilley-Kimball scheme ε_{ADK} combined with the Kasten–Czeplak sky cover scheme during all daylight periods, to be replaced with the Dilley & O'Brien Model B scheme ε_{CDO} during all nighttime hours (whether the night has a clear sky or not) rather than temporal gap-filling. Although the variance of the estimates derived this way remains lower than observed, the mean value is very consistently returned across both daily and seasonal cycles (Fig. 2).

4 Discussion

There is a wide variety of gap-filling techniques available for meteorological data (Falge et al. 2001; Xing et al. 2008), and many schemes have been designed for estimating L_d in particular (Brutsaert 1975; Prata 1996; Crawford and Duchon 1999; Niemelä et al. 2001; Iziomon et al. 2003; Flerchinger et al. 2009). Choosing the most appropriate for use is not a trivial issue because of the high importance of longwave fluxes in calculating canopy energy balances and many other ecosystem diagnostics (Monteith and Unsworth 1990; Leigh 1999; Jones et al. 2004). Having access to high-quality data from the flux tower at Caxiuanã, Eastern Pará, Brazil (Carswell et al. 2002; Iwata et al. 2005), we tested a variety of different emissivity-based schemes for estimating LW downward radiation in order to identify the best-performing scheme.

Air emissivity ε_a is a quantity that has been studied for many years (Tables 2 and 4). The first estimation schemes were proposed by Ångström (1915) and Brunt (1932) and assumed that εa increases simply with vapour pressure at reference height (equivalently, atmospheric precipitable water). Swinbank (1963) later demonstrated that ε_a also increases with screen temperature (Dilley and O'Brien 1998; Iziomon et al. 2003) and the work of Brutsaert (1975, 1982) combined these two trends into one scheme (the explicit decrease with Ta in the equation (Table 2) only has the effect of reducing the

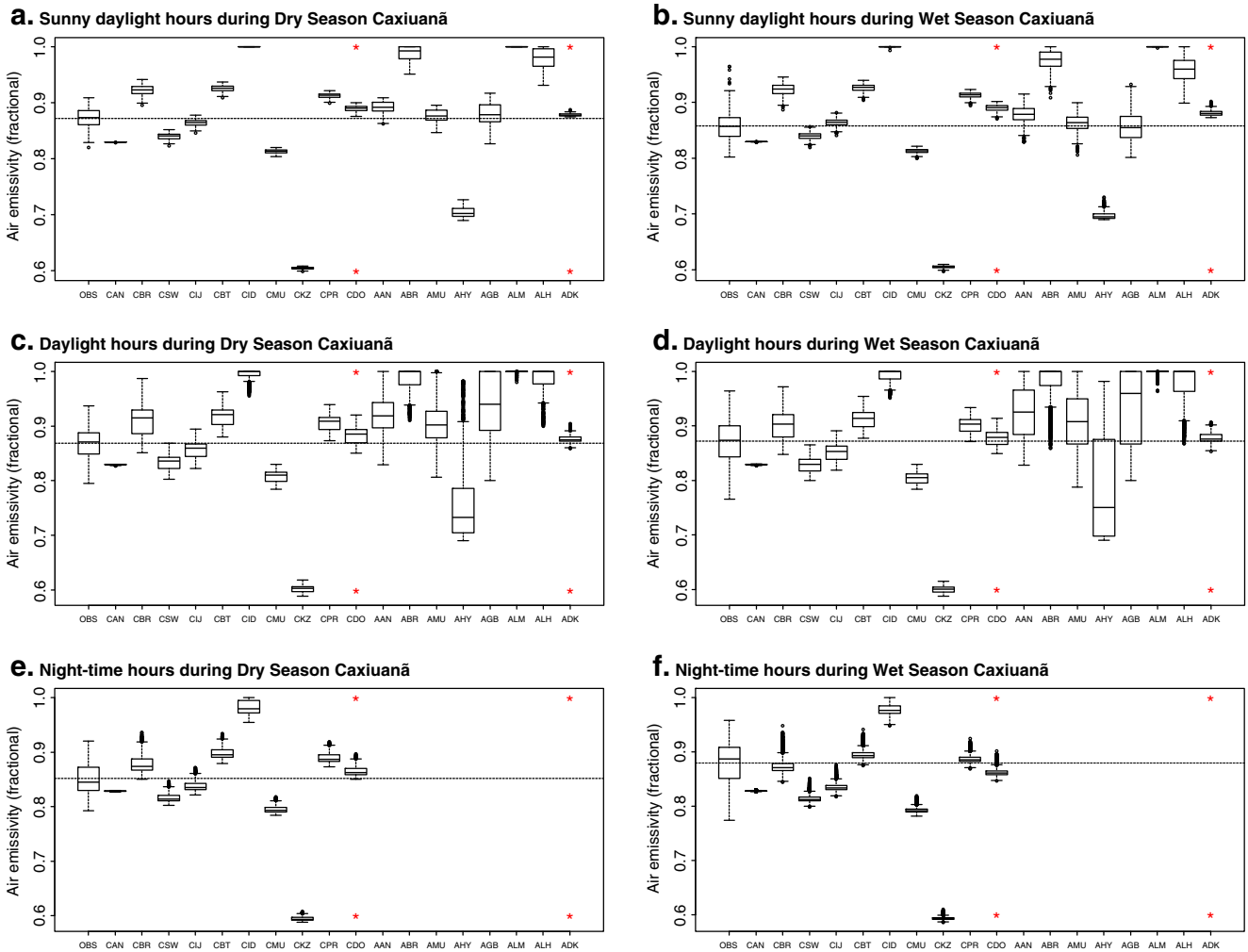

Fig. 2 Estimates of effective air emissivity, assuming the Kasten and Czeplak sky cover scheme (Table 3), for a lowland forest at Caxiuanã, Brazil, in the dry (**a**, **c**, **e**) and wet (**b**, **d**, **f**) seasons showing sunny daylight hours only (**a**, **b**), daylight hours only (**c**, **b**) and nighttime hours only (**e**, **f**). Estimates are from the schemes listed in Tables 2 and 4, with corresponding code on the horizontal axis (recommended schemes indicated by *asterisks*). Observed emissivity values from the Caxiuanã tower derived from measured longwave downward flux are displayed for comparison (OBS and the *horizontal broken line* showing the mean value of OBS). The Caxiuanã dry season was taken as 1st September to 30th November and the wet season as the rest of the year. Note that data points were divided into daylight and nighttime values based on positive solar elevation (calculated by *SolPos*; Rymes 1998), not by applying a threshold insolation value (e.g. Stöckli 2007). Sunny daylight hours were those data points with insolation H>750 W/m^2. Note that not all schemes could be evaluated at every time step (e.g. over the course of all measurements outside sensor breaks, temperature was available 100% but relative humidity only 57% of the time, so the means of schemes based on e, e.g. Brunt, Brutsaert, are means of fewer points than those based on T alone, e.g. Swinbank)

strong increase of e with Ta which happens as a result of the vapour pressure curve (see e.g. the Goff-Gratch equation, Hellwege & Madelung 1988), so on balance Brutsaert's equation does model a net increase of emissivity with Ta). Brutsaert's scheme probably remains the most widely-used even today, and is considered a more 'satisfactory' scheme because it may be derived theoretically (by assuming exponential atmospheric profiles for pressure, temperature and humidity, Lhomme et al. 2007). At Caxiuanã, Brazil - as at most locations worldwide - both temperature and precipitable water follow a similar daily cycle, increasing slowly during the day and returning to a steady value at night which appears to support this simple picture (note the similarity in shape between Swinbank's and Brutsaert's schemes, Fig. 3). Moving from the dry to the wet season, however, temperature decreases and precipitable water increases, and at Caxiuanã these lower canopy temperatures, which imply lower air temperatures just above the canopy (and therefore lower ε_a), appear to offset the precipitable water increase (acting to increase ε_a) and keep ε_a approximately constant (Fig. 2). A constant emissivity between seasons is only reliably predicted by a more sophisticated estimation schemes with a combined dependency on both temperature and precipitable water together (Tables 2 and 4).

At Caxiuanã, the Dilley-Kimball emissivity scheme (Kimball et al. 1982; Flerchinger et al. 2009) combined with Kasten and Czeplak (1980)'s sky cover scheme during the day and Dilley and O'Brien (1998)'s model B scheme at night proved to be the most reliable of those tested, yielding the most accurate estimates. These schemes have been found by others to be robust (Kimball et al. 1982; Dilley and O'Brien 1998; Flerchinger et al. 2009) and we suggest that this combination may be used more widely at least in similar bioclimatic zones in the tropics (Peel et al. 2007). This combination of Dilley-Kimball, Kasten-Czeplak and Dilley and O'Brien's model B unusually entails the use of different functional forms at diurnal and nocturnal time points (cf. Lhomme et al. 2007), but considering the behaviour of near-surface air masses, which are the transmission source for Ld, is well known to change greatly between diurnal and nocturnal hours (Iwata et al. 2005), this is not a surprising result (and even may be considered to have been anticipated by some comments by Ångström 1915 where he was uncertain whether "the effective temperature radiation during the day follows the same laws as hold for the nocturnal radiation", p. 75).

Surprisingly, several schemes designed for clear sky conditions actually predicted L_d less well at Caxiuanã under strictly clear sky conditions than their 'all-sky' counterparts (e.g. those of Ångström, and Monteith and Unsworth; Tables 2 and 3), and several schemes designed for clear sky conditions predicted L_d better at Caxiuanã than schemes designed for all-sky conditions even when conditions were not clear (notably Idso–Jackson; Table 2), which means that the division of these schemes between those for clear skies (Table 2) and those for all-sky conditions (Table 4) should be understood as one of intention only: A scheme derived for clear skies at one site may well be applicable at another site under cloudy conditions (as found for nocturnal hours at Caxiuanã here). This is simply a consequence of the semi-empirical nature of these relationships and the fact that they have been applied in this study at a site outside the bioclimatic range for which they were derived.

Emissivity estimation schemes do not generally return the greater variability clearly observed in real emissivity values (Fig. 2). Presumably, there are still functional dependencies not included in any of the estimation schemes considered here, and more work is required to elucidate

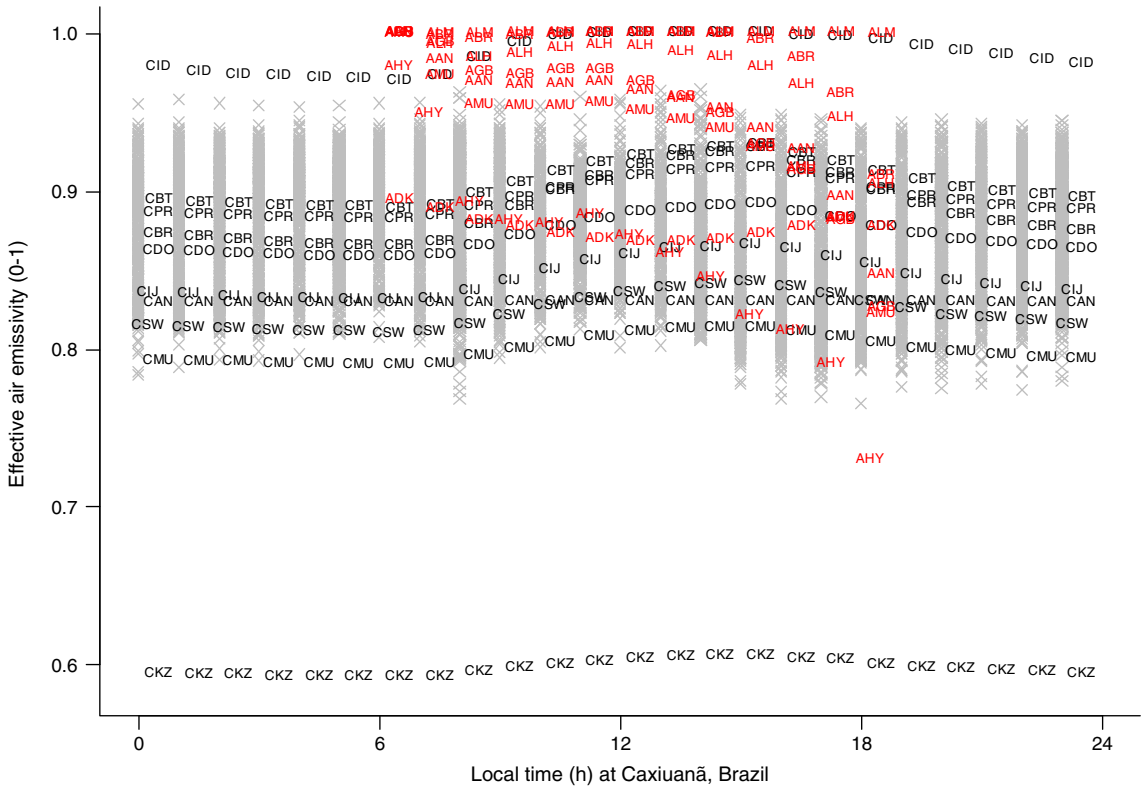

Fig. 3 The observed diurnal cycle of air emissivity measured at Caxiuanã, Brazil, during April 2002 to July 2003 (*grey x*, displaced 30 min earlier for clarity) and means for each hour of the corresponding estimate from all emissivity schemes (for codes and definitions, see Tables 2 and 4; clear sky schemes in *black*, all-sky schemes in *red*). It may be noticed that the Idso scheme (*CID*) is consistently high, as mentioned by Prata (1996), and the Konzelmann scheme (*CKZ*) consistently the lowest. Only mean values over all time points of each estimate are plotted without showing variation about the mean (±1SD was comparable to the size of the symbol for all except the all-sky schemes AAN, ABR, AMU, AHY, AGB and ALH)

what controls 'extreme values' of emissivity. The general lack of sensitivity of these emissivity schemes to sky cover implies that the sky cover schemes on which some of these depend are a potential source of error. Current sky cover schemes are based on simple measures of atmospheric clarity (Table 3) without detailed account being taken of cloud type, cloud base height or daily cloud cycles (e.g. stratiform clouds at altitude are less opaque than cumuliform clouds in the lowlands; Niemelä et al. 2001). An investigation of sub-daily cloud variation (which cannot be sampled by today's satellites; Table 1) at a wide variety of tropical sites (where cloudiness is relatively more important in controlling the radiation environment; Malhi et al. 2002b) is necessary to derive a more sophisticated sky cover scheme and, therefore, a better emissivity scheme. Regional atmospheric phenomena are also very significant, e.g. the quasi-permanent but non-precipitating stratiform cloud cover which occurs up to 800 km inland during the dry season in Gabon and Congo (Chapman et al. 1999), and the regional displacement of precipitation by the South American Low-Level Jet from Central Amazonia to the Río Plata Basin (Killeen 2007). These well known phenomena modify sky cover and emissivity relationships, and therefore vegetation dynamics, but these linkages remain poorly studied.

Looking ahead to the future, if air emissivity is a function of precipitable water, then longwave downward flux must also be linked fundamentally to the long-term El Niño cycles (Malhi and Wright 2004; Wright 2005). In the Amazon, El Niño teleconnections bring reduced cloud cover, mild drought and increased irradiance to NE Amazonia, whilst La Niña events bring the opposite (Malhi and Wright 2004; Wright 2005). The data for the current study covered the period of a weak La Niña 1999–2000 and a weak El Niño 2002–2003 (multivariate El Niño/Southern Oscillation index; http://www.esrl.noaa.gov/psd/enso/), so perhaps form a reasonable estimate of normal conditions, but if the frequency and severity of El Niño events increase in the future (Malhi and Wright 2004), then our analysis shows that this is likely to feed back via L_d into a markedly changed energy balance for the forest canopy at Caxiuanã. El Niño events seem generally to increase the release of forest CO_2 across the Amazon Basin (Killeen 2007), but in a warmer world, it is difficult to predict whether this will continue or perhaps reverse as a result of increased aerosol loads (e.g. from biomass burning; Lin et al. 2006; Kanniah et al. 2010). In order to address these issues and to really understand the causal links between regional-scale forcings and fine-scale forest canopy quantities such as energy and radiation balances, we need to understand much more precisely the mechanisms through which forests respond to environmental cues such as incoming radiation (Zelazowski et al. 2011).

We have found that the estimation schemes of Dilley and O'Brien, Kasten and Czeplak and Dilley–Kimball are adequate tools, in light of presently available data, for describing cloudiness effects at our lowland tropical forest site. Through their dependence on both temperature and precipitable water, they proved flexible enough to predict mean emissivity very well across all seasons at Caxiuanã. With the ever-increasing complexity of vegetation models and ecosystem simulations, it is becoming more essential to characterise the radiation environment and canopy energy balance correctly. We anticipate that these schemes will be used more widely as a result of this work, leading to improved modelling of vegetation dynamics in the eastern Amazon and other similar bioclimatic zones.

Acknowledgements This research was supported by Microsoft Research and the Oxford University John Fell Fund. We thank I. Perzia for all her extremely patient support and the staff of the Environmental Change Institute, University of Oxford, as well as C. Delire, A. Friend, P. Żelazowski, L. Cowley, P. Palmer, M. Allen, D. Andrews, H. Pumphrey, J. Wang, K. Halladay, P. Stier and two anonymous reviewers for useful comments during development of the text.

References

Allen RG, Pereira LS, Raes D, Smith M (1998) Crop evapotranspiration Guidelines for computing crop water requirements. FAO Irrigation and Drainage Paper 56, FAO, Rome, Italy. http://www.fao.org/docrep/X0490E/X0490E00.htm. Accessed 7 May 2011

Anderson ER (1954) Energy-budget studies. USGS Prof Pap 269:71–119

Ångström A (1915) A study of the radiation of the atmosphere. Smithsonian Miscellaneous Collections 65(3)

Ångström A (1924) Solar and terrestrial radiation. Q J Roy Meteor Soc 50:121–126

Aragão LEOC, Malhi Y, Metcalfe DB, Silva-Espejo JE, Jiménez E, Navarrete D, Almeida S, Costa ACL, Salinas N, Phillips OL, Anderson LO, Alvarez E, Baker TR, Goncalvez PH, Huamán-Ovalle J, Mamani-Solórzano M, Meir P, Monteagudo A, Patiño S, Peñuela MC, Prieto A, Quesada CA, Rozas-Dávila A, Rudas A, Silva JA, Vásquez R (2009) Above- and below-ground net primary productivity across ten Amazonian forests on contrasting soils. Biogeosciences 6:2759–2778

Avissar R, Nobre CA (2002) Preface to special issue on the Large-Scale Biosphere–Atmosphere Experiment in Amazonia (LBA). J Geophys Res D 107(D20):8034(LBA1)

Baldocchi D, Falge E, Gu LH, Olson R, Hollinger D, Running S, Anthoni P, Bernhofer C, Davis K, Evans R, Fuentes J, Goldstein A, Katul G, Law B, Lee XH, Malhi Y, Meyers T, Munger W, Oechel W, Paw UKT, Pilegaard K, Schmid HP, Valentini R, Verma S, Vesala T, Wilson K, Wofsy S (2001) FLUXNET: a new tool to study the temporal and spatial variability of ecosystem-scale carbon dioxide, water vapor, and energy flux densities. Bull Am Meteorol Soc 82:2415–2434

Berberan-Santos MN, Bodunov EN, Pogliani L (1997) On the barometric formula. Am J Phys 65:404–412

Bindi M, Miglietta F, Zipoli G (1992) Different methods for separating diffuse and direct components of solar radiation and their application in crop growth models. Clim Res 2:47–54

Bisht G, Bras RL (2010) Estimation of net radiation from the MODIS data under all sky conditions: Southern Great Plains case study. Remote Sens Environ 114:1522–1534

Black JN (1956) The distribution of solar radiation over the Earth's surface. Arch Meteor Geophy B 7:165–189
Brunt D (1932) Notes on radiation in the atmosphere I. Q J Roy Meteor Soc 58:389–420
Brutsaert W (1975) On a derivable formula for long-wave radiation from clear skies. Water Resour Res 11:742–744
Brutsaert W (1982) Evaporation into the atmosphere. D. Reidel, Dordrecht
Butt N, New M, Lizcano G, Malhi Y (2009) Spatial patterns and recent trends in cloud fraction and cloud-related diffuse radiation in Amazonia. J Geophys Res D 114:D21104
Campbell GS (1985) Soil physics with BASIC. Elsevier, Amsterdam
Campbell GS, Norman JM (1998) An introduction to environmental biophysics, 2nd edn. Springer, New York
Carswell FE, Costa AL, Palheta M, Malhi Y, Meir P, Costa JDR, Ruivo MD, Leal LDM, Costa JMN, Clement RJ, Grace J (2002) Seasonality in CO_2 and H_2O flux at an eastern Amazonian rain forest. J Geophys Res D 107:D8076
Chang J (1968) Climate and agriculture. Aldine, Chicago
Chapman CA, Gautier-Hion A, Oates JF, Onderdonk DA (1999) African primate communities: determinants of structure and threats to survival. In: Fleagle JG, Janson CH, Reed KE (eds) Primate communities. CUP, Cambridge, UK, pp. 1–37
Crawford TM, Duchon CE (1999) An improved parameterization for estimating effective atmospheric emissivity for use in calculating daytime downwelling longwave radiation. J Appl Meteorol 38:474–480
R Development Core Team (2011) R: a language and environment for statistical computing, version 2.12.1. R Foundation for Statistical Computing, Vienna. http://www.R-project.org. Accessed 7 May 2011
Dilley AC, O'Brien DM (1998) Estimating downward clear sky long-wave irradiance at the surface from screen temperature and precipitable water. Q J Roy Meteor Soc 124:1391–1401
Doorenbos J, Pruitt WO (1977) Crop water requirements. FAO Irrigation and Drainage Paper 24, FAO, Rome, Italy
Dubayah R, Rich PM (1995) Topographic solar radiation models for GIS. Int J Geogr Inf Syst 9:405–419
Dunne T, Leopold LB (1978) Water in environmental planning. W.H. Freeman, New York
Ellingson RG (1995) Surface longwave fluxes from satellite observations: a critical review. Remote Sens Environ 51:89–97
Falge E, Baldocchi D, Olson R, Anthoni P, Aubinet M, Bernhofer C, Burba G, Ceulemans R, Clement R, Dolman H, Granier A, Gross P, Grünwald T, Hollinger D, Jensen N, Katul G, Keronen P, Kowalski A, Lai CT, Law BE, Meyers T, Moncrieff J, Moors E, Munger JW, Pilegaard K, Rannik Ü, Rebmann C, Sukyer A, Tenhunen J, Tu K, Verma S, Vesala T, Wilson K, Wofsy S (2001) Gap filling strategies for defensible annual sums of net ecosystem exchange. Agr For Meteorol 107:43–69
Flerchinger GN, Xaio W, Marks D, Sauer TJ, Yu Q (2009) Comparison of algorithms for incoming atmospheric long-wave radiation. Water Resour Res 45:W03423
Friend AD (1998) Parameterisation of a global daily weather generator for terrestrial ecosystem modelling. Ecol Model 109:121–140
Friend AD (2001) Modelling canopy CO_2 fluxes: are 'big-leaf' simplifications justified? Glob Ecol Biogeogr 10:603–619
Friend AD, Stevens AK, Knox RG, Cannell MGR (1997) A process-based, terrestrial biosphere model of ecosystem dynamics (Hybrid v3.0). Ecol Model 95:249–287
Friend AD, Geider RJ, Behrenfeld MJ, Still CJ (2009) Photosynthesis in global-scale models. In: Laisk A, Nedbal L, Govindjee (eds) Photosynthesis in silico: understanding complexity from molecules to ecosystems. Springer, Dordrecht, pp 465–497
Gabathuler M, Marty CA, Hanselmann KW (2001) Parameterization of incoming longwave radiation in high-mountain environments. Phys Geogr 22:99–114
Gates DM (1980) Biophysical ecology. Springer, New York
Ghazoul J, Sheil D (2010) Tropical rain forest ecology, diversity, and conservation. Oxford University Press, Oxford
Goudriaan J (1977) Crop micrometeorology: a simulation study. Pudoc, Wageningen
Hellwege K, Madelung O (1988) Landolt–Börnstein numerical data and functional relationships in science and technology, volume V/4b: physical and chemical properties of the air. Springer, Berlin
Idso SB (1981) A set of equations for full spectrum and 8- to 14-μm and 10.5- to 12.5-μm thermal radiation from cloudless skies. Water Resour Res 17:295–304
Idso SB, Jackson RD (1969) Thermal radiation from the atmosphere. J Geophys Res 74:5397–5403
Ineichen P, Perez R (1999) Derivation of cloud index from geostationary satellites and application to the production of solar irradiance and daylight illuminance data. Theor Appl Climatol 64:119–130
Ineichen P, Perez R (2002) A new airmass independent formulation for the Linke turbidity coefficient. Sol Energy 73:151–157
Intergovernmental Panel on Climate Change (2007) Climate Change 2007: the Fourth IPCC Assessment Report. Cambridge University Press, Cambridge
Iqbal M (1983) An introduction to solar radiation. Academic, Toronto
Ivanov VY, Bras RL, Curtis DC (2007) A weather generator for hydrological, ecological, and agricultural applications. Water Resour Res 43:W10406
Iwata H, Malhi Y, von Randow C (2005) Gap-filling measurements of carbon dioxide storage in tropical rainforest canopy airspace. Agr For Meteorol 132:305–314
Iziomon MG, Mayer H, Matzarakis A (2003) Downward atmospheric longwave irradiance under clear and cloudy skies: measurement and parameterization. J Atmos Sol-Terr Phy 65:1107–1116
Jegede OO, Ogolo EO, Aregbesola TO (2006) Estimating net radiation using routine meteorological data at a tropical location in Nigeria. Int J Sustain Energy 25:107–115
Jones HG, Archer N, Rotenberg E (2004) Thermal radiation, canopy temperature and evaporation from forest canopies. In: Mencuccini M, Grace J, Moncrieff J, McNaughton KG (eds) Forests at the land–atmosphere interface. CABI Publishing, Wallingford, pp 123–144
Kanniah KD, Beringer J, Tapper NJ, Long CN (2010) Aerosols and their influence on radiation partitioning and savanna productivity in northern Australia. Theor Appl Climatol 100:423–438
Kasten F, Czeplak G (1980) Solar and terrestrial radiation dependent on the amount and type of cloud. Sol Energy 24:177–189
Killeen TJ (2007) A perfect storm in the Amazon wilderness. Advances in Applied Biodiversity Science 7. http://www.conservation.org/publications/pages/perfect_storm.aspx. Accessed 7 May 2011
Kimball BA, Idso SB, Aase JK (1982) A model of thermal radiation from partly cloudy and overcast skies. Water Resour Res 18:931–936
Konzelmann T, van de Wal RSW, Greuell W, Bintanja R, Henneken EAC, Abe-Ouchi A (1994) Parameterization of global and longwave incoming radiation for the Greenland Ice Sheet. Glob Planet Chang 9:143–164
Kotarba AZ (2010) Estimation of fractional cloud cover for moderate resolution imaging spectroradiometer/Terra cloud mask classes with high-resolution over ocean ASTER observations. J Geophys Res D 115:D22210
Landsberg J, Sands P (2011) Physiological ecology of forest production. Academic, Amsterdam
Leigh EG (1999) Tropical climates. In: Leigh EG (ed) Tropical forest ecology: a view from Barro Colorado Island. Oxford University Press, New York, pp 46–66
Lewis SL, Lloyd J, Sitch S, Mitchard ETA, Laurance WF (2009) Changing ecology of tropical forests: evidence and drivers. Annu Rev Ecol Evol S 40:529–549

Lhomme JP, Vacher JJ, Rocheteau A (2007) Estimating downward long-wave radiation on the Andean Altiplano. Agr For Meteorol 145:139–148

Lin JC, Matsui T, Pielke RA, Kummerow C (2006) Effects of biomass-burning-derived aerosols on precipitation and clouds in the Amazon Basin: a satellite-based empirical study. J Geophys Res D 111:D19204

Lisboa PLB (1997) A Estação Científica Ferreira Penna/ECFPn. In: Lisboa PLB (ed), Caxiuanã, Museu Paraense Emílio Goeldi, Belém, Brazil, pp 20–49

Liu BYH, Jordan RC (1960) The interrelationship and characteristic distribution of direct, diffuse, and total solar radiation. Sol Energy 4:1–19

Malhi Y (2010) The carbon balance of tropical forest regions, 1990–2005. Curr Opin Environ Sustain 2:237–244

Malhi Y, Wright J (2004) Spatial patterns and recent trends in the climate of tropical rainforest regions. Philos Trans R Soc B 359:311–329

Malhi Y, Meir P, Brown S (2002a) Forests, carbon and global climate. Philos Trans R Soc A 360:1567–1591

Malhi Y, Pegoraro E, Nobre AD, Pereira MGP, Grace J, Culf AD, Clement R (2002b) Energy and water dynamics of a central Amazonian rain forest. J Geophys Res 107(D20):LBA45

Malhi Y, Aragão LEOC, Metcalfe DB, Paiva R, Quesada CA, Almeida S, Anderson L, Brando P, Chambers JQ, da Costa ACL, Hutyra LR, Oliveira P, Patiño S, Pyle EH, Robertson AL, Teixeira LM (2009) Comprehensive assessment of carbon productivity, allocation and storage in three Amazonian forests. Glob Chang Biol 15:1255–1274

Martínez-Lozano JA, Tena F, Onrubia JE, de la Rubia J (1984) The historical evolution of the Ångström formula and its modifications: review and bibliography. Agr For Meteorol 33:109–128

Mercado LM, Huntingford C, Gash JHC, Cox PM, Jogireddy V (2007) Improving the representation of radiation interception and photosynthesis for climate model applications. Tellus B 59:553–565

Mercado LM, Bellouin N, Sitch S, Boucher O, Huntingford C, Wild M, Cox PM (2009) Impact of changes in diffuse radiation on the global land carbon sink. Nature 458:1014–1018

Mokhov II, Akperov MG (2006) Tropospheric lapse rate and its relation to surface temperature from reanalysis data. Izvestiya Atmos Ocean Phys 42:430–438

Monteith JL, Unsworth MH (1990) Principles of environmental physics, 2nd edn. Butterworth, Oxford

Muneer T, Gueymard C, Kambezidis H (2004) Solar radiation and daylight models, 2nd edn. Elsevier Butterworth-Heinemann, Oxford

Niemelä S, Räisänen P, Savijärvi H (2001) Comparison of surface radiative flux parameterizations. Part I: Longwave radiation. Atmos Res 58:1–18

Okogbue EC, Adedokun JA, Holmgren B (2009) Hourly and daily clearness index and diffuse fraction at a tropical station, Ile-Ife, Nigeria. Int J Climatol 29:1035–1047

Peel MC, Finlayson BL, McMahon TA (2007) Updated world map of the Köppen–Geiger climate classification. Hydrol Earth Syst Sc 11:1633–1644

Penman HL (1948) Natural evaporation from open water, bare soil and grass. P Roy Soc Lond A 193:120–146

Perez R, Ineichen P, Seals R, Zelenka A (1990) Making full use of the clearness index for parameterizing hourly insolation conditions. Sol Energy 45:111–114

Pirazzini R, Nardino M, Orsini A, Calzolari F, Georgiadis T, Levizzani V (2000) Parameterization of the downward longwave radiation from clear and cloudy skies at Ny Ålesund (Svalbard). In: Smith WL, Timofeyev YM (eds) International Radiation Symposium (IRS) July 2000, St Petersburg, Russia: Current Problems in Atmospheric Radiation. Deepak Publishing, Hampton, Virginia, pp 559–562

Prata AJ (1996) A new long-wave formula for estimating downward clear-sky radiation at the surface. Q J Roy Meteor Soc 122:1127–1151

Prentice IC, Bondeau A, Cramer W, Harrison SP, Hickler T, Lucht W, Sitch S, Smith B, Sykes MT (2007) Dynamic global vegetation modeling: quantifying terrestrial ecosystem responses to large-scale environmental change. In: Canadell JG, Pataki DE, Pitelka LF (eds) Terrestrial ecosystems in a changing world. Springer, Berlin, pp 175–192

Rose F, Charlock T, Wielicki B, Doelling D, Zentz S (2006) CERES synoptic gridded diurnaly resolved radiative transfer. Proceedings of the 12th Conference on Atmospheric Radiation, Madison, WI, USA, 10–14 July. http://ams.confex.com/ams/pdfpapers/112517.pdf. Accessed 7 May 2011

Ross J (1975) Radiative transfer in plant communities. In: Monteith JL (ed) Vegetation and the atmosphere (vol. I). Academic, London, pp 13–55

Rossow WB, Schiffer RA (1991) ISCCP cloud data products. Bull Am Meteorol Soc 72:2–20

Rossow WB, Mosher F, Kinsella E, Arking A, Desbois M, Harrison E, Minnis P, Ruprecht E, Seze G, Simmer C, Smith E (1985) ISCCP cloud algorithm intercomparison. J Clim Appl Meteorol 24:877–903

Rymes M (1998) The SolPos algorithm. National Renewable Energy Laboratory, USA. http://rredc.nrel.gov/solar/codesandalgorithms/solpos. Accessed 7 May 2011

Şen Z (2008) Solar energy fundamentals and modeling techniques. Springer, London

Spitters CJT, Toussaint HAJM, Goudriaan J (1986) Separating the diffuse and direct component of global radiation and its implications for modeling canopy photosynthesis. Part I. Components of incoming radiation. Agr For Meteorol 38:217–229

Stöckli R (2007) LBA-MIP driver data gap filling algorithms. Unpublished. http://www.climatemodeling.org/lba-mip/LBAmipDriverDataFillingMethods.pdf. Accessed 7 May 2011

Suits GH (1972) The calculation of the directional reflectance of a vegetative canopy. Remote Sens Environ 2:117–125

Swinbank WC (1963) Long-wave radiation from clear skies. Q J Roy Meteor Soc 89:339–348

Walsh RPD (1996) Climate. In: Richards PW, Walsh RPD, Baillie IC, Greig-Smith P (eds) The tropical rain forest, 2nd edn. Cambridge University Press, Cambridge, pp 159–205, 503–540

Weishampel JF, Urban DL (1996) Coupling a spatially-explicit forest gap model with a 3-D solar routine to simulate latitudinal effects. Ecol Model 86:101–111

Wild M (2008) Short-wave and long-wave surface radiation budgets in GCMs: a review based on the IPCC-AR4/CMIP3 models. Tellus A 60:932–945

Wright SJ (2005) The El Niño Southern Oscillation influences tree performance in tropical rainforests. In: Bermingham E, Dick CW, Moritz C (eds) Tropical rainforests: past, present, and future. University of Chicago Press, Chicago, pp 295–310, 611–713

Xing Z, Bourque CP, Meng F, Cox RM, Swift DE, Zha T, Chow L (2008) A process-based model designed for filling of large data gaps in tower-based measurements of net ecosystem productivity. Ecol Model 213:165–179

Zelazowski P, Malhi Y, Huntingford C, Sitch S, Fisher JB (2011) Changes in the potential distribution of humid tropical forests on a warmer planet. Philos Tr R Soc A 369:137–160